Spatial Quantification of Cytosolic Ca^{2+} Accumulation in Nonexcitable Cells: An Analytical Study

Fernando López-Caamal, Diego A. Oyarzún, Richard H. Middleton, and Míriam R. García

Abstract—Calcium ions act as messengers in a broad range of processes such as learning, apoptosis, and muscular movement. The transient profile and the temporal accumulation of calcium signals have been suggested as the two main characteristics in which calcium cues encode messages to be forwarded to downstream pathways. We address the analytical quantification of calcium temporal-accumulation in a long, thin section of a nonexcitable cell by solving a boundary value problem. In these expressions we note that the cytosolic Ca^{2+} accumulation is independent of every intracellular calcium flux and depends on the Ca^{2+} exchange across the membrane, cytosolic calcium diffusion, geometry of the cell, extracellular calcium perturbation, and initial concentrations. In particular, we analyse the time-integrated response of cytosolic calcium due to i) a localised initial concentration of cytosolic calcium and ii) transient extracellular perturbation of calcium. In these scenarios, we conclude that i) the range of calcium progression is confined to the vicinity of the initial concentration, thereby creating calcium microdomains; and ii) we observe a low-pass filtering effect in the response driven by extracellular Ca^{2+} perturbations. Additionally, we note that our methodology can be used to analyse a broader range of stimuli and scenarios.

Index Terms—Intracellular calcium dynamics, nonlinear reaction-diffusion systems, astrocytes, exact analytical solution, Ca^{2+} microdomains

1 Introduction

Calcium ions (Ca^{2+}) are the most ubiquitous secondary messenger mediating a large number of cellular functions, such as cell growth and differentiation, membrane excitability, and cell death [1], [2]. To regulate multiple Ca^{2+}-dependent signalling cascades, cells have evolved complex homoeostatic mechanisms that control both dynamics and location of cytosolic calcium concentration ($[Ca^{2+}]_c$). These mechanisms work at different time and length scales and may be classified in three categories: Ca^{2+} influx, Ca^{2+} buffering, and internal Ca^{2+} storage [3].

A delicate interplay of these processes allows multiple Ca^{2+} signalling cascades to be regulated independently within the same cell. Some Ca^{2+}-triggered processes depend on the continuous presence of elevated cytosolic Ca^{2+} or just require certain Ca^{2+} load to trigger specific downstream mechanism [4], while other Ca^{2+}-dependent processes are regulated separately through distinct signalling pathways linked to specific routes/locations of Ca^{2+} influx [3]. For example it is known that the duration and extent of Ca^{2+}-influx may determine whether a cell survives, dies by apoptosis, or undergoes necrosis [5]. Here excessive Ca^{2+} load mediates the activation of various cytosolic hydrolytic enzymes (such as calpains implicated in toxic cell death in the liver), ischemic damage, excitotoxic neuronal damage [3], [6], and mitochondrial damage with the subsequent release of cytochrome-c, SMAC, and other protein factors related to apoptotic death [4], [7]. However, the complexity of biochemical reactions networks and transport phenomena at different time and length scales usually hinder our understanding of how Ca^{2+} ions selectively activate and modulate downstream pathways.

To overcome this difficulty, *in silico* analyses have been useful as forecast tools or hypotheses test-beds to study the role of Ca^{2+} signalling in a wide variety of conditions and prominent diseases, such as ageing [8], cardiac diseases [9], or neurodegenerative disorders [10]. Unfortunately, in these simulation-based studies it is unclear whether predictions are a consequence of the parameter values used for simulation or a consequence of a structural property of the studied system. As an alternative, models may be simplified so they become tractable by analytical methods and, thus, one can study the structural properties of the underlying biological system. In the rest of this paper, we opt for the later analytical approach.

A balanced simplification of the reaction-diffusion models is challenging, since both temporal and spatial distribution are essential. In this context, many examples in the literature study analytical solutions of systems which only exhibit wave propagation (see, e.g., [11] and references therein) and, thus, only deal with spatial effects. In contrast,

- *F. López-Caamal is with the Hamilton Institute, National University of Ireland, Maynooth, Co. Kildare, Ireland. E-mail: fernando.lopezcaamal.2009@nuim.ie.*
- *D. A. Oyarzún is with the Department of Mathematics, Imperial College London, London SW7 2AZ, United Kingdom. E-mail: d.oyarzun@imperial.ac.uk.*
- *R. H. Middleton is with the Centre for Complex Dynamic Systems and Control, The University of Newcastle, Callaghan, New South Wales, Australia 2308. E-mail: Richard.Middleton@newcastle.edu.au.*
- *M. R. García is with the Process Engineering Group, IIM-CSIC, Spanish National Research Council, Vigo, Pontevedra, Spain. E-mail: miriamr@iim.csic.es.*

Manuscript received 10 Oct. 2013; revised 10 Feb. 2014; accepted 19 Mar. 2014. Date of publication 6 Apr. 2014; date of current version 5 June 2014. For information on obtaining reprints of this article, please send e-mail to: reprints@ieee.org, and reference the Digital Object Identifier below. Digital Object Identifier no. 10.1109/TCBB.2014.2316010

only a few works analyse systems with transient characteristics in a spatial domain, for instance in protein cascades [12], in tissue drug degradation [13], and in skeletal muscle growth [14].

In order to analytically quantify the calcium load, in this work we derive spatially distributed time-integrals of cytosolic calcium concentration, $c_c(t,x)$, with respect to their resting level, $c_c^*(x)$, which we denote as the *$[Ca^{2+}]_c$ accumulation*:

$$I(c_c)(x) := \int_0^\infty \big(c_c(t,x) - c_c^*(x)\big)\,\mathrm{d}t. \tag{1}$$

$[Ca^{2+}]_c$ accumulation has been considered as a mechanism to encode messages to downstream pathways as noted in [4], [15]. In addition, experimentally measured *$[Ca^{2+}]_c$ accumulation* has been used to assess the strength and location of the response in cytosolic calcium due to different stimuli such as extracellular cues in [16]; Ca^{2+} dynamics in dendrites [17]; correlation between intracellular Ca^{2+} increase and dilated cardiomyopathic myocardium [18]; and to implicate Ca^{2+} uptake with neuron necrosis after ischemic damage [19]. In fact, the quantification of time-integrated responses was proposed in [20], where the authors used a time-integral to discover an amplification effect in the MAPK pathway.

We base our study on the model in [21] and adopt biologically motivated assumptions, which allow us to rewrite the integral above as the analytical solution of a boundary value problem (BVP). We note that these conditions are mild and allow us to compute the *$[Ca^{2+}]_c$ accumulation* under the presence of nonlinearities representing different calcium fluxes in a thin and long nonexcitable cell.

In Section 3, we tackle this problem with two different approaches: $i)$ by obtaining the Green's function of the BVP and $ii)$ by means of the Laplacian Decomposition Method (a type of projection method often employed to handle PDEs) [22], [23]. We refer the interested reader to [24], [25] for more details on general conditions for the computation of the integrated response in a class of nonlinear reaction-diffusion systems.

1.1 Nonexcitable Cells

Neurons are cells capable of reacting to electrical stimuli; to propagate them; and interact with surrounding neurons. This communication is supported by a group of voltage-inert cells (nonexcitable cells) denoted glial cells. A member of this family is the astrocyte, which is the most abundant cell in the human brain.

Astrocytes play a major role by insulating axons; controlling blood flow; and providing energy and neurotransmiters to motivate signal transmission. In fact, malfunction of Ca^{2+} regulation might be implicated in epilepsy [26]. In addition, astrocytes may become cancerous, hence leading to gliomas or can be affected by autoimmune attacks in multiple sclerosis [27], [28].

In contrast to neurons or neuroendocrine cells, mature astrocytes lack voltage-gated Ca^{2+} channels [29] and are unable to generate action potentials. Instead, they sense neuronal activity by increasing Ca^{2+} intracellular levels in response to ligand binding and 1, 4, 5-trisphosphate (IP_3) mediated mobilisation of Ca^{2+} from intracellular stores [30]. This phenomenon is denoted Ca^{2+} excitability. Subsequent increases in intracellular Ca^{2+} from endoplasmic stores elicit gliotransmitter release such as glutamate, ATP and D-serine. This bidirectional communication between neurons and astrocytes has been denoted as "tripartite synapse."

Although early evidence of bidirectional communication between neurons and astrocytes goes back to 1990s, the "tripartite synapse" still is an active research topic. One of the main reasons is the spatial heterogeneity observed in the distribution of astrocytic Ca^{2+} [31]. This intracellular Ca^{2+} heterogeneity depends greatly on the area and layer of the brain. For instance, $[Ca^{2+}]_c$ microdomains depend on the characteristics of the neuronal input in cerebellum [32], whereas amplitude of $[Ca^{2+}]_c$ in astrocytes in hippocampal CA1 region is correlated with the number of simultaneously activated synapses. In addition, Ca^{2+} microdomains have been implicated in mechanisms controlling cellular process, such as the release of gliotransmitters [30], [32].

In this paper, we derive mathematical expressions to quantify the *$[Ca^{2+}]_c$ accumulation* for a long, thin astrocyte dendrite. We avail of these formulae as a proxy to identify Ca^{2+} microdomains due to localised initial concentrations of cytosolic Ca^{2+} (Section 4.1). Additionally, we assess the effect of extracellular Ca^{2+} spatio-temporal perturbation in cytosolic Ca^{2+} concentration (Section 4.2).

2 Spatially Distributed Model for Ca^{2+} Import and Storage

We base our study on a mechanistic model describing Ca^{2+} fluxes to and from the cytosol, along with diffusion of cytosolic Ca^{2+}. This model is a modified version of that described in [21, Ch. 7, p. 305]. In this section, we first describe the original model and the additional biological assumptions we consider. Later, in Section 2.2 we show that its resting (i.e., equilibrium) concentrations are spatially homogeneous.

2.1 Model Description

Cytosolic Ca^{2+} homoeostasis results from the interaction of biochemical reactions and fluxes through different organelles and the cellular membrane. The main fluxes are depicted in Fig. 1. There we show the processes by which Ca^{2+} enters the cell (J_{in}) through open Ca^{2+} ion channels depending mainly on inositol 1, 4, 5-trisphosphate (IP_3). We also show how Ca^{2+} ions are expelled (J_{out}) by Ca^{2+} pumps, usually combined with Na^+/Ca^{2+} exchangers. Ca^{2+} ions are pumped into the sarcoplasmic/endoplasmic reticulum (ER) by means of Ca^{2+} pumps (J_{serca}) and released through IP_3 receptors (J_{IPR}) or ryanodine receptors (J_{RyR}). In addition, Ca^{2+} can be buffered by different proteins either endogenous, such as calmodulin, or exogenous buffers added to measure the quantity of Ca^{2+} (J_{on} and J_{off}).

In recent years, there have been many efforts to define mathematical models able to represent the main spatio-temporal progression of $[Ca^{2+}]_c$. A well-known model was developed by Keener and Sneyd [21, Ch. 7, p. 305], which assumes intertwined cytoplasmic and endoplasmic reticulum spaces and a long, thin cylindrical cell. In addition, it

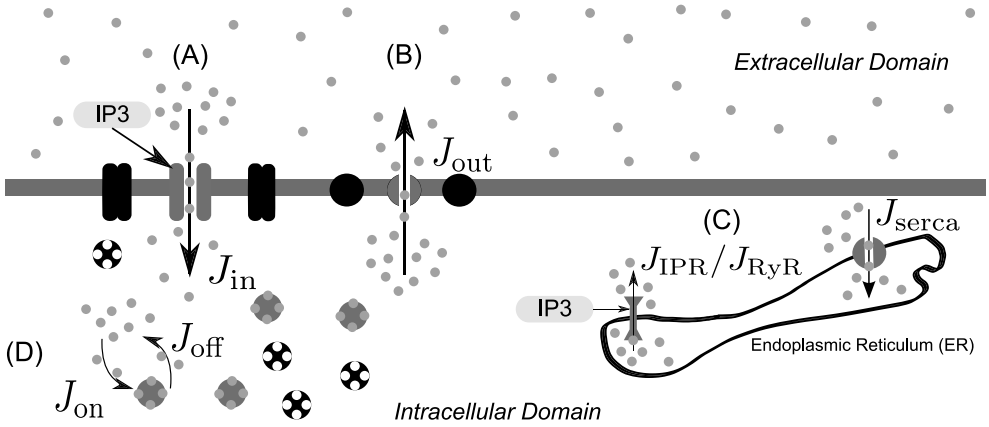

Fig. 1. Main Ca^{2+} fluxes in a nonexcitable cell. (A) depicts the IP_3-mediated influx of Ca^{2+} to the intracellular domain (J_{in}); whereas (B) represents the efflux of $[Ca^{2+}]_c$ due to membrane pumps (J_{out}) triggered by the presence of Na^+ (not shown); (C) shows the fluxes of Ca^{2+} to/from the Endoplasmic or Sarcoplasmic Reticulum (J_{serca} and J_{IPR} or J_{RyR}). Ca^{2+} buffering flux (J_{on}) and its release from the buffers (J_{off}) are shown in (D).

considers influx and pumped Ca^{2+} fluxes across the membrane J_{in} and J_{out}, respectively:

$$\frac{\partial}{\partial t}c_c = D_c\frac{\partial^2 c_c}{\partial x^2} + J_{\text{IPR}} + J_{\text{RyR}} - J_{\text{serca}} + \frac{\rho}{A}(J_{\text{in}} - J_{\text{out}}) - J_{\text{on}} + J_{\text{off}} + J_{\text{pert}}, \tag{2a}$$

$$\frac{\partial}{\partial t}c_e = D_e\frac{\partial^2 c_c}{\partial x^2} - \gamma\big(J_{\text{IPR}} + J_{\text{RyR}} - J_{\text{serca}}\big) - J_{\text{on,e}} + J_{\text{off,e}}; \tag{2b}$$

with the appropriate initial conditions and subject to the boundary conditions

$$\frac{\partial c_c}{\partial x} = \frac{\partial c_e}{\partial x} = 0, \qquad \text{at } x = 0 \text{ and } x = L. \tag{2c}$$

Here c_c and c_e are the Ca^{2+} concentrations in the cytosol and ER; whereas L, ρ, A and γ represent geometrical parameters of the cell (length, circumference, cross-sectional area, and the ratio of cytoplasmic to ER volumes, respectively). The constants D_c and D_e denote the cytosolic Ca^{2+} and ER Ca^{2+} diffusivity, respectively. Furthermore, the fluxes $J_{\text{on,e}}$ and $J_{\text{off,e}}$ represent the buffering mechanism within the ER. We additionally include a perturbation flux J_{pert} in the model, representing transient spatial perturbations of extracellular Ca^{2+}. This type of spatial whole-cell model in which the cytosolic and ER coexist are often referred to as "bidomain" models, and are commonly used to study Ca^{2+} homoeostasis (see [33], for example).

The full model can be complemented with kinetic expressions for the import and buffering fluxes, leading to a nonlinear PDE that is typically intractable with analytical methods. To tackle this difficulty, we incorporate the following additional biological observations into the model:

1. *Dominant cytosolic diffusion.* The spatial dynamics are dominated by cytosolic diffusion. We thus assume a negligible diffusion coefficient within the ER. This is a standard assumption [21], and even in those models that consider diffusion within the ER, it is assumed that it is negligible compared to its cytosolic counterpart (i.e., $D_e \ll D_c$).
2. *Calcium buffering due to immobile buffers.* Buffering of $[Ca^{2+}]_c$ is mainly carried out by immobile buffers in the cytosol. It has been shown that only ~1-5 percent of Ca^{2+} in the cytosol is free and ~75 percent of total cytoplasmic buffers are immobile [34]. The cytoplasmic buffers are either large proteins, such as calmodulin, with low diffusion coefficients or are anchored to the cytoskeleton and membrane [35, Ch. 1]. In addition, since Ca^{2+} buffering in the ER is negligible compared to cytosolic buffering, the majority of models in the literature assume that $J_{\text{on,e}} = J_{\text{off,e}} = 0$ (see, e.g., [21], [33], [36]). We also consider that the only process that affects the buffer concentration is its turnover, i.e., neither the buffer nor the Ca^{2+}-buffer complex interact with other pathways (or they do it in different spatio-temporal scales or locations). Under these assumptions, the concentration of free buffers, b, can be described by
$$\frac{\partial}{\partial t}b = -J_{\text{on}} + J_{\text{off}}, \tag{3}$$
with the Ca^{2+}-buffer complexes given by $b_{\text{T}} - b$, where b_{T} denotes the sum of free and bound buffer molecular concentrations.
3. *Linear calcium cycling across the membrane.* We assume that Ca^{2+} cycling across the cellular membrane is an affine function of $[Ca^{2+}]_c$. Although this is generally a valid assumption when modelling Ca^{2+} influx, see for example [36], this might not be accurate enough when modelling Ca^{2+} efflux carried out by the joint effect of Ca^{2+} pumps and Na^+/Ca^{2+} exchangers. This is usually the case for excitable cells and most non-excitable cells, as other non-excitable cells might employ only Ca^{2+} pumps [37]. In these cases the efflux is usually modelled via Michaelis-Menten or Hill kinetics. However, it is commonly assumed that Ca^{2+} pumps present high affinity and low capacity for Ca^{2+}, in contrast to Na^+/Ca^{2+} exchangers, with low affinity and high capacity [6], [38]. Due to the difference in capacity, pump efflux is usually small compared to exchanger efflux. Hence this flux can be considered affine in Ca^{2+} (see the experimental

results in [39]). That is, we assume the functional form $J_{\text{out}} = k_e c_c + k_p$. With this approximation, the cycling of Ca^{2+} across the membrane can then be expressed as

$$\frac{\rho}{A}(J_{\text{in}} - J_{\text{out}}) = -\alpha c_c + \beta, \tag{4}$$

for some $\alpha, \beta > 0$.

Under the three assumptions above the model in (2) takes the following form:

$$\begin{aligned}\frac{\partial}{\partial t}c_c = D_c\frac{\partial^2 c_c}{\partial x^2} + J_{\text{IPR}} + J_{\text{RyR}} - J_{\text{serca}} - J_{\text{on}} + J_{\text{off}} \\ + J_{\text{pert}} - \alpha c_c + \beta,\end{aligned} \tag{5a}$$

$$\frac{\partial}{\partial t}c_e = -\gamma\big(J_{\text{IPR}} + J_{\text{RyR}} - J_{\text{serca}}\big), \tag{5b}$$

$$\frac{\partial}{\partial t}b = -J_{\text{on}} + J_{\text{off}}, \tag{5c}$$

subject to the boundary conditions

$$\frac{\partial c_c}{\partial x} = \frac{\partial c_e}{\partial x} = \frac{\partial b}{\partial x} = 0, \qquad \text{at } x = 0 \text{ and } x = L. \tag{6}$$

Although this model is not as general as (2), it comprises a large variety of scenarios that align with the biological assumptions above, including cases with highly nonlinear intracellular fluxes or, even, when their mathematical formulations are unknown. In the following section we will obtain the steady state concentrations of (5) and show that the only admissible equilibrium for c_c is homogeneous in the spatial coordinate.

2.2 Resting Levels of the System

We denote the resting levels (i.e., the steady state concentrations) of the respective species as c_c^*, c_e^* and b^*, which satisfy

$$\frac{\partial c_c^*(x,t)}{\partial t} = \frac{\partial c_e^*(x,t)}{\partial t} = \frac{\partial b^*(x,t)}{\partial t} = 0. \tag{7}$$

Note that the only diffusing state is $c_c(x,t)$, and that the spatial distributions of the remaining species depend on this field. Since the perturbation J_{pert} is transient, we have that $\lim_{t\to\infty} J_{\text{pert}} = 0$ and thus from the model (5) we get the following boundary value problem for the resting level of cytosolic Ca^{2+}:

$$D_c\frac{\partial^2 c_c^*(x)}{\partial x^2} - \alpha c_c^*(x) + \beta = 0, \ \left.\frac{\partial c_c^*(x)}{\partial x}\right|_{x=0,L} = 0. \tag{8}$$

In the absence of diffusion, the stationary concentration of $[Ca^{2+}]_c$ is β/α. This suggests the following functional form for the resting level of cytosolic calcium

$$c_c^*(x) = \frac{\beta}{\alpha} + w(x), \tag{9}$$

where $w(x)$ is a function that represents the spatial distribution of the steady state. Therefore, the boundary value problem in (8) can be reduced to

$$D_c\frac{\partial^2 w(x)}{\partial x^2} - \alpha w(x) = 0, \text{ subject to } \left.\frac{\partial w(x)}{\partial x}\right|_{x=0,L} = 0. \tag{10}$$

To find an analytical solution for (10) we use the Laplacian Spectral Decomposition method [22], [23]. This method is based upon the assumption that the spatially distributed function $w(x)$ belongs to a Hilbert space, hence admitting a series expansion of the form

$$w(x) \approx \sum_{i=1}^{n} \phi_i(x) m_i, \tag{11}$$

where $\phi_i(x)$, $i \in [1,n]$, are the elements of the spatial basis of the Hilbert space and m_i, $i \in [1,n]$ are the coefficients or weights of each basis element. We note than when $n = \infty$, (11) is exact. The elements in $\{\phi_i(x)\}_{i=1}^n$ are orthonormal; invariant w.r.t. the Laplacian operator, as required by the Laplacian Spectral Decomposition Method; and subject to the boundary conditions described in (10). That is

$$\begin{aligned}\frac{\partial^2 \phi_i(x)}{\partial x^2} = -\lambda_i \phi_i(x), \ \forall\, i = 1, 2, \ldots, n, \\ \text{subject to } \left[\frac{\partial \phi_i(x)}{\partial x}\right]_{x=0,L} = 0.\end{aligned} \tag{12}$$

In the case of a unidimensional domain $\Omega = [0, L]$, a set of eigenfunctions and eigenvalues is given by

$$\lambda_i = \left[(i-1)\frac{\pi}{L}\right]^2, \tag{13a}$$

$$\phi_i(x) = k_i \frac{1}{\sqrt{L}} \cos\left((i-1)\frac{\pi}{L}x\right), \tag{13b}$$

where

$$k_i = \begin{cases} 1, & \text{if } i = 1, \\ \sqrt{2}, & \text{if } i \neq 1. \end{cases}$$

By combining equations (10)-(12), we get

$$\sum_{i=1}^{\infty} D_c \lambda_i \phi_i(x) m_i = \sum_{i=1}^{\infty} -\alpha \phi_i(x) m_i,$$

which projected over the basis functions and exploiting its orthonormality (i.e., $\int_0^L \phi_i \phi_j \mathrm{d}x = \delta_{ij}$ with δ_{ij} being the Kronecker delta) leads to

$$(D_c\lambda_i + \alpha) m_i = 0, \ \forall\, i = 1, 2, \ldots, n. \tag{14}$$

We see that provided $\alpha \neq -D_c[(i-1)\pi L]^2$, $\forall\, i$ the only solution to (10) is $m_i = 0$, $\forall\, i = 1, 2, \ldots, \infty$. As per our assumption 3 in Section 2.1, $\alpha > 0$ and, hence this condition is always satisfied. This implies that $w(x) = 0$, and therefore the resting level of cytosolic calcium is unique, spatially homogeneous, and given by

$$c_c^* = \frac{\beta}{\alpha}. \tag{15}$$

The resting levels of the remaining species, i.e., buffer and Ca^{2+} concentration in the ER, depend on the buffer binding kinetics and cycling through the ER. Hence, they need to be computed with particular fluxes describing the buffering and cycling through the ER. We will further assume that these are also unique and homogeneous. By defining the deviation variables (relative to the resting levels)

$$e_c = c_c - c_c^*, \tag{16a}$$

$$e_e = c_e - c_e^*, \tag{16b}$$

$$e_b = b - b^*, \tag{16c}$$

we can rewrite the model (5) as

$$\begin{aligned}\frac{\partial}{\partial t}e_c = D_c\frac{\partial^2 e_c}{\partial x^2} + J_{\text{IPR}} + J_{\text{RyR}} - J_{\text{serca}} \\ - J_{\text{on}} + J_{\text{off}} + J_{\text{pert}} - \alpha e_c + \beta,\end{aligned} \tag{17a}$$

$$\frac{\partial}{\partial t}e_e = -\gamma(J_{\text{IPR}} + J_{\text{RyR}} - J_{\text{serca}}), \tag{17b}$$

$$\frac{\partial}{\partial t}e_b = -J_{\text{on}} + J_{\text{off}}, \tag{17c}$$

subject to the boundary conditions

$$\frac{\partial e_c}{\partial x} = \frac{\partial e_e}{\partial x} = \frac{\partial e_b}{\partial x} = 0, \text{ at } x = 0 \text{ and } x = L. \tag{18}$$

Here the buffer binding kinetics and cycling fluxes now depend on the respective deviation coordinates and resting levels. In the forthcoming section we derive the analytical expressions for $[Ca^{2+}]_c$ *accumulation*.

3 Analytic Derivation of the $[Ca^{2+}]_c$ Accumulation

We now focus on deriving a general analytic formulae for the $[Ca^{2+}]_c$ *accumulation* based on the reaction-diffusion model of the previous section. In order to compute these integrals the key observation is that in the model (17) an auxiliary variable defined as

$$q(t,x) := e_c(t,x) + \gamma^{-1}e_e(t,x) - e_b(t,x), \tag{19}$$

satisfies the following linear PDE

$$\frac{\partial}{\partial t}q(t,x) = D_c\frac{\partial^2}{\partial x^2}e_c(t,x) - \alpha e_c(t,x) + J_{\text{pert}}(t,x). \tag{20}$$

Integrating (20) from $t = 0$ to $t = \infty$ we obtain

$$\begin{aligned}-q(0,x) = \int_0^\infty D_c\frac{\partial^2}{\partial x^2}e_c(t,x)\,\mathrm{d}t - \int_0^\infty \alpha e_c(t,x)\,\mathrm{d}t \\ + \int_0^\infty J_{\text{pert}}(t,x)\,\mathrm{d}t.\end{aligned} \tag{21}$$

By swapping the integral and Laplacian operators in the first term of the r.h.s. of the equation above we obtain

$$-\frac{\mathrm{d}^2}{\mathrm{d}x^2}\{I(c_c)(x)\} + \theta^2 I(c_c)(x) = f(x), \tag{22a}$$

$$\frac{\mathrm{d}}{\mathrm{d}x}I(c_c)(0) = \frac{\mathrm{d}}{\mathrm{d}x}I(c_c)(L) = 0, \tag{22b}$$

where $I(c_c)(x)$ is the $[Ca^{2+}]_c$ *accumulation* defined in (1) and

$$\theta := \sqrt{\frac{\alpha}{D_c}}, \tag{23a}$$

$$f(x) := D_c^{-1}\left(q(0,x) + \int_0^\infty J_{\text{pert}}(t,x)\,\mathrm{d}t\right). \tag{23b}$$

The boundary conditions in (22b) arise, in turn, from the no-flux boundary conditions in (6) of the original problem.

The differential equation in (22) is a linear, second order, ordinary boundary value problem. We will proceed in two different ways to obtain the solution for $I(c_c)(x)$. The first approach is based on obtaining the Green's function $g(x,\xi)$ of this BVP. From this perspective we will be able to derive exact close-form solutions for $I(c_c)(x)$, whenever the convolution of $f(x)$ and $g(x,\xi)$, as described below, can be readily computed. In the second approach, we avail of the LSD method to express the solution of $I(c_c)(x)$ as an infinite series in terms of the eigenfunctions of the spatial domain $\{\phi_i(x)\}_{i=1}^\infty$ in (13). This approach is useful, when an analytical solution cannot be easily obtained by the previous approach or when $f(x)$ in (23b) is expressed in terms of the eigenfunctions of the spatial domain.

3.1 Green's Function Approach

In this first approach, we will derive a solution to (22) by means of the Green's function associated with the relevant homogeneous differential operator [40]. That is to say, for a Green's function $g(x,\xi)$ that satisfies

$$-\frac{\partial^2}{\partial x^2}g(x,\xi) + \theta^2 g(x,\xi) = \delta(x-\xi), \tag{24a}$$

$$\frac{\partial}{\partial x}g(0,\xi) = \frac{\partial}{\partial x}g(L,\xi) = 0, \tag{24b}$$

where $\delta(x-\xi)$ is the Dirac delta. In turn, the solution for $I(c_c)(x)$ in (22) due to the forcing term $f(x)$ in (23b) is given by

$$I(c_c)(x) = \int_0^L g(x,\xi)f(\xi)\mathrm{d}\xi. \tag{25}$$

In Appendix A we show that, for our problem, $g(x,\xi)$ in (24) has the form

$$\begin{aligned}g(x,\xi) = \frac{1}{\theta\sinh(\theta L)} \\ \times\begin{cases}\cosh(\theta[\xi - L])\cosh(\theta x), & 0 \le \xi < x, \\ \cosh(\theta\xi)\cosh(\theta[x - L]), & x \le \xi \le L.\end{cases}\end{aligned} \tag{26}$$

Moreover, when the forcing term $f(x)$ in (25) is symmetric with respect to the centre of the spatial domain, i.e., $L/2$, the solution for $I(c_c)(x)$ is symmetric. In this case, we can obtain the symmetric solution for $I(c_c)(x)$ by replacing L with $L/2$ in (26) and in (24b), as the choice for L was arbitrary during the derivation of $g(x,\xi)$ in Appendix A. Summarising, when $f(x)$ is symmetric with respect of the axis $x = L/2$, the solution for (24a) $x \in [0, L/2]$ is

$$g_s(x,\xi) = \frac{1}{\theta \sinh\left(\theta \frac{L}{2}\right)} \times \begin{cases} \cosh\left(\theta[\xi - \frac{L}{2}]\right) \cosh\left(\theta x\right), & 0 \le \xi < x, \\ \cosh\left(\theta \xi\right) \cosh\left(\theta[x - \frac{L}{2}]\right), & x \le \xi \le \frac{L}{2}. \end{cases} \quad (27)$$

Therefore, the solution for $I(c_c)(x)$ in (22) is given by

$$I(c_c)(x) = \int_0^{L/2} g_s(x,\xi) f(\xi) \mathrm{d}\xi, \quad 0 \le x \le \frac{L}{2}, \quad (28a)$$

$$I(c_c)(x - L/2) = I(c_c)(L/2 - x), \quad 0 \le x \le L. \quad (28b)$$

When a closed form solution to (28a) cannot be easily obtained, it is still possible to obtain a solution in terms of an infinite series as described in the forthcoming section.

3.2 LSD Approach

In this approach, as in Section 2.2, we rewrite each field of the model (17) in terms of time-dependent coefficients and spatial basis functions:

$$e_j(t,x) = \sum_{i=1}^{\infty} \phi_i(x) m_i^j(t), \text{ for } j \in \{c, e, b\}. \quad (29)$$

The *$[Ca^{2+}]_c$ accumulation* defined in (1) becomes

$$I(c_c)(x) = \int_0^{\infty} e_c(t,x)\, \mathrm{d}t = \sum_{i=1}^{\infty} \phi_i(x) \int_0^{\infty} m_i^c(t)\, \mathrm{d}t, \quad (30)$$

and therefore the *$[Ca^{2+}]_c$ accumulation* can be computed from the integrals of the coefficients m_i^c. These integrals can be computed by expressing $e_c(t,x)$ in (21) by its series representation and then project it on each of the basis functions. From this procedure the integral of the coefficients $m_i^c(t)$ are

$$\int_0^{\infty} m_i^c(t)\, \mathrm{d}t = \frac{m_i^f}{\lambda_i + \theta^2}, \quad (31)$$

where λ_i are the eigenvalues of the Laplacian operator as in (13a),

$$m_i^f := D_c^{-1} \left(m_i^c(0) + \gamma^{-1} m_i^e(0) - m_i^b(0) + \int_0^{\infty} m_i^g(t)\, \mathrm{d}t \right), \quad (32)$$

and m_i^g are the coefficients of J_{pert} (i.e., $J_{\text{pert}}(t,x) = \sum_{i=0}^{\infty} \phi_i(x) m_i^g(t)$). Substituting (31) back into (30) we get the following expression for the *$[Ca^{2+}]_c$ accumulation*:

$$I(c_c)(x) = \sum_{i=1}^{\infty} \phi_i(x) \frac{m_i^f}{\lambda_i + \theta^2}. \quad (33)$$

The Green's function in (26) and the expression (33), obtained with the LSD method, indicate that *$[Ca^{2+}]_c$ accumulation* depends only on:

- the cycling terms proportional to $[Ca^{2+}]_c$ through the cellular membrane collected in α and the Ca^{2+} diffusivity D_c, both included in the term θ defined in (23a),
- the boundary conditions and spatial geometry inherent to the solution of the Green's function in (26) (or explicitly comprised in $\phi_i(x)$ and λ_i),
- the initial conditions and resting values, and the total inflow of extracellular Ca^{2+} contained in the perturbation $J_{\text{pert}}(t,x)$ and contained in the term $f(x)$ in (23b) or its expansion m_i^f in (32).

This analysis suggests that the *$[Ca^{2+}]_c$ accumulation* is independent of the buffering and cycling through the ER. Therefore, any Ca^{2+}-dependent downstream cascade activated only by the *$[Ca^{2+}]_c$ accumulation* is independent of other intracellular processes, while these processes can modulate or trigger other downstream cascades. In the next section we use the results in this section to quantify the impact of different types of perturbations on the *$[Ca^{2+}]_c$ accumulation* in non-excitable cells.

4 *$[Ca^{2+}]_c$ Accumulation* in Non-Excitable Cells

In this section, we make use of a mathematical model inspired on the one in [36], to study the *$[Ca^{2+}]_c$ accumulation* in different example biological scenarios. There, the authors defined the Ca^{2+} fluxes as

$$J_{\text{IPR}} + J_{\text{RyR}} = k_1(T + T_0)(c_e - c_c), \quad (34a)$$

$$J_{\text{on}} = k_2 c_c b, \quad (34b)$$

$$J_{\text{off}} = k_{m2}(b_{\text{T}} - b), \quad (34c)$$

$$J_{\text{serca}} = V_3 \frac{c_c^2}{k_4^2 + c_c^2}, \quad (34d)$$

$$J_{\text{in}} = k_5(T + T_0)(c_{\text{out}} - c_c), \quad (34e)$$

$$J_{\text{out}} = V_6 \frac{c_c^2}{k_7^2 + c_c^2}. \quad (34f)$$

Definitions and values for the constants can be found in [36, (pp. 660-662)] and are repeated in Table 1 for convenience.

With the definition of Ca^{2+} fluxes as defined in (34) and considering a bidomain model in a long, thin cell we can express the model in (5) as

$$\begin{aligned} \frac{\partial}{\partial t} c_c =& D_c \frac{\partial^2 c_c}{\partial x^2} + k_1(T + T_0)(c_e - c_c) \\ & - V_3 \frac{c_c^2}{k_4^2 + c_c^2} - k_2 c_c b + k_{m2}(b_{\text{T}} - b) \\ & + \frac{\rho}{A} \left(k_5(T + T_0)(c_{\text{out}} - c_c) - V_6 \frac{c_c^2}{k_7^2 + c_c^2} \right), \end{aligned} \quad (35a)$$

TABLE 1
Parameters Definition of the Model (35), Taken from [36]

Parameter	Definition	Value
k_1	Rate of calcium release form the store	$7.5[\mathrm{s}^{-1}]$
k_2	Rate of calcium association with the buffer	$601[(\mu\mathrm{M\ s})^{-1}]$
k_{m2}	Rate of calcium dissociation from the buffer	$97[\mathrm{s}^{-1}]$
V_3	Maximum rate of calcium pumping into the store	$500[\mu\mathrm{M/s}]$
k_4	Dissociation constant of the store calcium pump	$0.1[\mu\mathrm{M}]$
k_5	Rate of calcium influx from the external medium	$0.000158[\mathrm{s}^{-1}]$
V_6	Maximum rate of the plasma membrane pump	$1.5[\mu\mathrm{M/s}]$
k_7	Dissociation constant of the plasma membrane pump	$0.6[\mu\mathrm{M}]$
c_{out}	Extracellular calcium concentration	$1500[\mu\mathrm{M}]$
b_{tot}	Total concentration of the calcium buffer	$300[\mu\mathrm{M}]$
T_0	Basal fractional activity of the channels in the store	$0.2[1]$
T	Fractional activity of the channels in the store	$0.8[1]$

$$\frac{\partial}{\partial t}c_e = \gamma\left(-k_1(T+T_0)(c_e-c_c)+V_3\frac{c_c^2}{k_4^2+c_c^2}\right), \tag{35b}$$

$$\frac{\partial}{\partial t}b = -k_2c_cb+k_{m2}(b_{\mathrm{T}}-b), \tag{35c}$$

subject to the boundary conditions in (6). Korngreen's model uses a unique Hill equation to simulate the Ca^{2+} extrusion ($V_6\frac{c_c^2}{k_7^2+c_c^2}$) representing the Ca^{2+} pump without any Na^+/Ca^{2+} exchangers nor Ca^{2+} leak. However, we note that for the range $[Ca^{2+}]_c \in [0.1, 0.6][\mu\mathrm{M}]$ the characteristic of the pump may be approximated by the following affine function in $[Ca^{2+}]_c$

$$V_6\frac{c_c^2}{k_7^2+c_c^2} \approx k_ec_c-k_p. \tag{36}$$

Here $k_e = 1.4953[\mathrm{s}^{-1}]$ and $k_p = 0.1396[\mu\mathrm{M/s}]$ are obtained for the linearisation of the pump characteristic around c_c^*. By substituting (36) in (35a) we have

$$\begin{aligned}\frac{\partial}{\partial t}c_c = {} & D_c\frac{\partial^2 c_c}{\partial x^2}+k_1(T+T_0)(c_e-c_c)\\ & -V_3\frac{c_c^2}{k_4^2+c_c^2}-k_2c_cb+k_{m2}(b_{\mathrm{T}}-b)\\ & +\frac{\rho}{A}\big(k_5(T+T_0)(c_{\mathrm{out}}-c_c)-k_ec_c+k_p\big),\end{aligned} \tag{37a}$$

$$\frac{\partial}{\partial t}c_e = \gamma\left(-k_1(T+T_0)(c_e-c_c)+V_3\frac{c_c^2}{k_4^2+c_c^2}\right), \tag{37b}$$

$$\frac{\partial}{\partial t}b = -k_2c_cb+k_{m2}(b_{\mathrm{T}}-b), \tag{37c}$$

subject to the boundary conditions in (6). We note that by letting

$$\alpha = \frac{\rho}{A}(k_5(T+T_0)+k_e), \tag{38a}$$

$$\beta = \frac{\rho}{A}\big(k_5(T+T_0)c_{\mathrm{out}}+k_p\big), \tag{38b}$$

defined in (4), we can express the PDE set in (37) as the general model in (5) and the $[Ca^{2+}]_c$ *accumulation* can be computed by means of (33).

In the following, we will analytically derive and study the $[Ca^{2+}]_c$ *accumulation* in astrocytes by studying Ca^{2+} accumulation in two different scenarios: a localised initial concentration of cytosolic $Ca^{2+}$and a spatio-temporal perturbation of extracellular Ca^{2+}.

4.1 Localised Initial Concentration of $[Ca^{2+}]_c$

Proteins buffer Ca^{2+} more rapidly than these ions are sequestrated by the endoplasmatic reticulum. The former scatters elevated Ca^{2+} along the spatial domains, whereas the latter prolongs the duration of the Ca^{2+} signal in a particular location [34], resulting in what it is usually called biphasic response. Moreover, buffering proteins are usually categorised depending on their capacity to diffuse. Here we will focus on immobile buffers and their effect on $[Ca^{2+}]_c$ since 75 percent of total cytoplasmic buffers cannot diffuse [34]. For a study of mobile Ca^{2+} buffers we refer the interested reader to [41], where an effective diffusion is derived as a function of Ca^{2+} and buffer concentrations.

TABLE 2
Geometric and Additional Kinetic Parameters for the Model (37)

Parameter	Definition	Value	Reference
k_e	Slope of the Ca pump	$1.4953[\mathrm{s}^{-1}]$	Equation (36)
k_p	Bias term of the linearisation of the Ca pump	$0.1396[\mu\mathrm{M/s}]$	Equation (36)
d	Cytoplasmic diffusion constant for Ca^{2+}	$250[\mu\mathrm{m}^2/\mathrm{s}]$	[41]
γ	Ratio of cytoplasmic to ER volumes	$0.167[1]$	[33]
L	Length of the cylindrical cell	$100[\mu\mathrm{m}]$	Fig. 2B in [42]
r	Radius of cylindrical cell	$0.5[\mu\mathrm{m}]$	Fig. 2C in [42]
ρ	Circumference of cylindrical cell	$2\pi r[\mu\mathrm{m}]$	
A	Cellular cross sectional area	$\pi r^2[\mu\mathrm{m}^2]$	

Immobile buffers tend to immobilise Ca^{2+} in localised areas of a cell. The main function of this immobilization is to confine Ca^{2+} and avoid triggering unwanted signalling routes [30]. The influence of these kind of buffers is particularly relevant to regulation of the redistribution of Ca^{2+} entering the cell by ion channels via diffusion [41]. We study these Ca^{2+} microdomains by assessing the response of an initial condition of $[Ca^{2+}]_c$ representing entry of Ca^{2+} through membrane ion-channels. We model this initial profile as a square pulse centred in the spatial domain. This profile can be mathematically expressed in terms of the step function $h(\circ)$ as

$$c_c(0,x) = c_c^* + \psi\left[h\left(x - \left(\frac{L}{2} - \varepsilon\right)\right) - h\left(x - \left(\frac{L}{2} + \varepsilon\right)\right)\right]. \tag{39}$$

Here 2ε is the width of the square pulse, whereas ψ represent its magnitude. By assuming the rest of the species in equilibrium at $t = 0$ and no perturbation of $[Ca^{2+}]_c$ (i.e., $J_{\text{pert}} = 0$), the forcing term $f(x)$ in (22a) becomes

$$f(x) = \frac{\psi}{D_c}\left[h\left(x - \left(\frac{L}{2} - \varepsilon\right)\right) - h\left(x - \left(\frac{L}{2} + \varepsilon\right)\right)\right], \tag{40}$$

which is a symmetric function w.r.t. the axis $x = L/2$. Hence we use the Green's function in (27) to obtain $I(c_c)(x)$. This solution is

$$I(c_c)(x) = \frac{\psi}{\alpha} \times \begin{cases} 1 - \frac{\sinh(\theta[L/2-\varepsilon])}{\sinh(\theta L/2)}\cosh\left(\theta\left[x - \frac{L}{2}\right]\right), & \left|x - \frac{L}{2}\right| \le \varepsilon, \\ \varrho\cosh\left(\theta\left[\left|x - \frac{L}{2}\right| - \frac{L}{2}\right]\right), & \left|x - \frac{L}{2}\right| > \varepsilon, \end{cases} \tag{41}$$

where

$$\varrho = \frac{1}{\cosh\left(\theta\left[\frac{L}{2} - \varepsilon\right]\right)}\left[1 - \frac{\sinh\left(\theta\left[\frac{L}{2} - \varepsilon\right]\right)}{\sinh\left(\theta\frac{L}{2}\right)}\cosh(\theta\varepsilon)\right]. \tag{42}$$

The details of this derivation are in Appendix B. We note that $I(c_c)(x)$ is proportional to the magnitude of the initial pulse of $[Ca^{2+}]_c$ (i.e., ψ) and inversely proportional to the cycling fluxes of Ca^{2+} through the cellular membrane in the term α. In addition, the semi-width of the pulse, ε, determines the size of the magnitude of $I(c_c)(x)$ as described in the definition of ϱ in (42).

Fig. 2 shows that the progression of Ca^{2+} is confined to a vicinity of the original location of the initial concentration. Consequently, every physiological event triggered by this initial Ca^{2+} spatial distribution will be located close to the original location of the initial condition. This supports the observation that Ca^{2+} acts locally, having multiple spatially segregated Ca^{2+} subdomains [35, Ch. 2]. In addition, this approach can be used to determine the spatial extension of this Ca^{2+} initial stimulus. Of note, the activity localisation is specially relevant not only in Ca^{2+} astrocytes [32], but in exocitotoxic Ca^{2+} overload in neurons, where a subpopulation of mitochondria are damaged by Ca^{2+} overload due to a localised increases in $[Ca^{2+}]_c$ [43]. In the following section

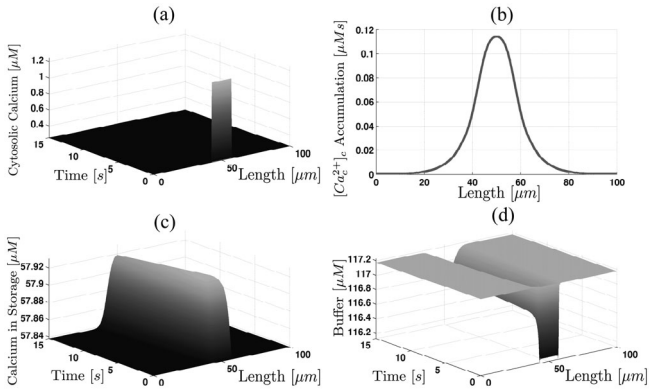

Fig. 2. Spatiotemporal and time-integrated response to a localised initial $[Ca^{2+}]_c$ stimulus. Panel (a) represents the cytosolic calcium response due to the initial $[Ca^{2+}]_c$ concentration in (39), whereas panel (b) shows the integrated $[Ca^{2+}]_c$ response in (41); in turn panels (c) and (d) show the spatiotemporal concentrations of the calcium in storage and buffer, respectively. The kinetic parameters are given in Tables 1 and 2; in addition, $\varepsilon = 7.5$ [μm] and $\psi = 1$ [μM].

we consider the effect of extracellular spatiotemporal perturbations of $[Ca^{2+}]_c$ on *$[Ca^{2+}]_c$ accumulation*.

4.2 Spatio-Temporal Perturbation of Extracellular Ca^{2+}

Extracellular Ca^{2+} may modulate cellular functions, such as dentinogenesis (formation of dentin, a substance that forms the majority of teeth) in odontoblasts [44] or cell fusion and growth on myoblasts [45]. In addition, there exist evidence suggesting that extracellular Ca^{2+} can be involved in cell death by intoxication [46]. In these experiments, cumene hydroperoxide seems to induce an influx of extracellular Ca^{2+}, which leads to spatially heterogeneous disturbances in $[Ca^{2+}]_c$. Moreover, in astrocytes extracellular Ca^{2+} changes may depend on other astrocytes and neurons relying on Ca^{2+}-voltaged channels to generate their action potentials [10].

With our previous results in Section 3, we will derive an analytical formula for *$[Ca^{2+}]_c$ accumulation* under spatially heterogeneous influx of Ca^{2+} and determine whether it translates into a localised increase of $[Ca^{2+}]_c$. To this end, we consider the response due to spatial and temporal anisotropies of extracellular Ca^{2+} (c_{out}). Suppose that several cells release calcium close enough of the modelled astrocyte, and that the extracellular Ca^{2+} perturbation may be represented by

$$c_{\text{out}} = \overline{c}_{\text{out}} + \nu\exp(-\kappa_1 t)\cos\left(\left[\kappa_2 - 1\right]\frac{\pi}{L}x\right), \tag{43}$$

here $\overline{c}_{\text{out}}$ denotes the constant unperturbed extracellular Ca^{2+} concentration, whereas the second term in (43) represents a temporal transient fluctuation. When the effect of the perturbation has vanished, $c_c(t)$ will eventually return to c_c^*. The constant ν in (43) is the initial magnitude of the perturbation; κ_1 represents the perturbations temporal decay rate; and κ_2 defines the frequency of the cosine function in (43). The profile for $c_{\text{out}}(t,x)$ in (43) leads to a perturbation term J_{pert} in (20) of the form

$$J_{\text{pert}}(t,x) = \kappa_0 \exp(-\kappa_1 t)\cos\left([\kappa_2 - 1]\frac{\pi}{L}x\right), \qquad (44)$$

where $\kappa_0 := \rho k_5 (T + T_0)\nu / A$. The space-integral of J_{pert} can be easily expressed in terms of the orthonormal basis (13). In this representation the coefficients for $J_{\text{pert}}(t,x)$ are

$$m_i^g(t) = \kappa_0 \frac{\sqrt{L}}{k_i}\exp(-\kappa_1 t)\delta_{\kappa_2,i},$$

where $\delta_{\kappa_2,i}$ denotes the Kronecker delta. Integrating the foregoing expression with respect to time yields

$$\int_0^\infty m_i^g(t)\,\mathrm{d}t = \frac{\kappa_0}{\kappa_1}\frac{\sqrt{L}}{k_i}\delta_{\kappa_2,i}.$$

By assuming all the species concentrations are initially in equilibrium, the coefficients of the forcing function $f(x)$ in (32) are $m_i^f = D_c^{-1}\int_0^\infty m_i^g(t)\,\mathrm{d}t$ and, from (33), the analytical expression for *$[Ca^{2+}]_c$ accumulation* becomes

$$\begin{aligned} I(c_c)(x) &= \sum_{i=1}^{\infty}\frac{k_i}{\sqrt{L}}\frac{1}{D_c}\frac{\cos\left((i-1)\frac{\pi}{L}x\right)}{\left[(i-1)\frac{\pi}{L}\right]^2 + \alpha/D_c}\int_0^\infty m_i^g(t)\,\mathrm{d}t \\ &= \frac{1}{D_c}\frac{\kappa_0}{\kappa_1}\frac{1}{\omega_{\kappa_2}^2 + \alpha/D_c}\cos\left(\omega_{\kappa_2}x\right), \end{aligned} \qquad (45)$$

where $\omega_{\kappa_2} := \left[(\kappa_2 - 1)\frac{\pi}{L}\right]$. We note that the factor multiplying the cosine function above is a monotonically decreasing function of the modal frequency ω_{κ_2}. This suggests a low-pass filtering effect of spatial 'noise', which may prevent the accidental triggering of downstream physiological events by fast stochastic fluctuations. As is common in frequency domain analysis, the magnitude of the cosine function in (45) will decrease slowly until the cut-off frequency $\sqrt{\alpha/D_c}$. As the value of ω_{κ_2} increases beyond this value, the term $(\omega_{\kappa_2}^2 + \alpha/D_c)^{-1}$ will rapidly decrease. That is, if

$$\kappa_2 + 1 \gg \frac{\theta}{\pi}L,$$

the perturbation flux $J_{\text{pert}}(t,x)$ will be filtered out. Finally, we note that the time integral in (45) is inversely proportional to the decay rate κ_1 of the perturbation term $J_{\text{pert}}(t,x)$ in (44); that is to say, if κ_1 has a large value, then $J_{\text{pert}}(t,x)$ vanishes quickly and, hence, $I(c_c)(x)$ in (45) is small.

Fig. 3 shows the spatiotemporal and accumulated response due to the perturbation of $c_{\text{out}}(t,x)$ in (43). There, we note that although having an intricate transient response, the *$[Ca^{2+}]_c$ accumulation* is a sinusoidal, the amplitude of which is closely related by (45) to the spatial frequency of the extracellular promoting signal.

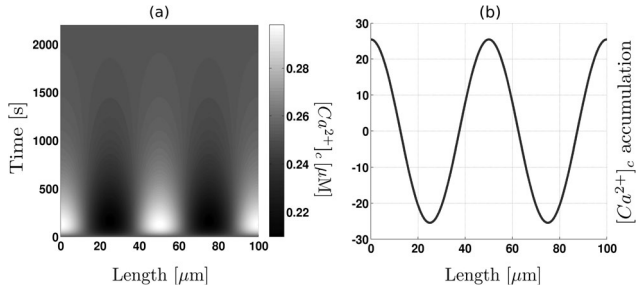

Fig. 3. $[Ca^{2+}]_c$ response in (37), due to the sinusoidal spatiotemporal perturbation of extracellular calcium, c_{out}, in (43), and initial conditions in equilibrium. Panel (a) depicts the cytosolic calcium $[Ca^{2+}]_c$ progression in time and space, whereas panel (b) shows the time integral of this progression (45). The additional parameters for simulation are $\nu = 1{,}000$, $\{\kappa_0, \kappa_1, \kappa_2\} = \{\frac{\rho}{A}(k_5\nu[T+T_0]), 0.0025, 5\}$.

5 Discussion and Concluding Remarks

Ca^{2+} cues are of paramount relevance as they trigger a large variety of physiological phenomena, some of which may determine cellular fate. For example, malfunction of glutamate or Ca^{2+} release in the astrocyte-mediated synapses [47] has been implicated in simultaneous neuronal firing underlying epileptic seizures [26]. In mice, downregulation of the apoptotic process in neurons and astrocytes leads to the appearance of tumours termed gliomas [48]. Although Ca^{2+} can trigger apoptosis, the thresholds of Ca^{2+} that lead to cellular damage depend on the cell type and pathological conditions [6]. This suggests the existence of tight regulatory mechanisms that modulate the Ca^{2+} progression in time and space. To understand these spatiotemporal patterns, cytosolic calcium concentration has been measured using different indicators such as Fura-2. Experimental technologies, such as photon counting multispectral video microscopy combined with calcium aequorin indicator, allow us to get accurate data of cytosolic calcium spatiotemporal concentrations [49]. We consider that mathematical models can be a powerful tool to interpret such data and shed light on cellular regulatory mechanisms. In this work, we focused on the derivation of analytical formulae that describe the *$[Ca^{2+}]_c$ accumulation* in astrocytes; and further analysed them to determine its relationship with cellular processes. The assumptions and predictions derived from this theoretical study could potentially be validated using these experimental techniques.

For our analysis, we have used a modified version of Keener's model [21]. The assumptions we adopted (Section 2.1) are that

- Ca^{2+} diffusion is dominated by diffusion in the cytosol;
- all relevant buffers are immobile; and
- the cycling of Ca^{2+} through the membrane can be approximated by an affine function on $[Ca^{2+}]_c$.

Assumptions 1 and 2 are supported by experimental evidence [21], [33], [34], [35], [36] and are widely adopted in the available models. The main limitation of our model is the validity of Assumption 3, as usually membrane calcium pumps follow Michaelis-Menten or Hill kinetics. Our model is valid in cases where pumps have high affinity and low capacity for calcium ions, as typically considered for calcium pumps [6], [37], [38]. In this case, we may approximate the dynamics by a function affine in cytosolic calcium concentration. Assumption 3 is also valid when the concentrations are close to the resting Ca^{2+} levels, even when the characteristic of the pumps are nonlinear.

To analyse *$[Ca^{2+}]_c$ accumulation*, we first characterised the resting state of $[Ca^{2+}]_c$. For a unidimensional spatial domain with no-flux boundary conditions and

spatially-homogeneous parameters, this equilibrium is unique and spatially-homogeneous. Moreover, this equilibrium point is solely a function of the constants describing the linear Ca^{2+} cycling across the cellular membrane. It is important to note that for different boundary conditions or even when some parameters are spatially distributed the resting state of $[Ca^{2+}]_c$ is not longer homogeneous. In these cases, we suggest the use of the Laplacian Spectral Decomposition method to estimate the $[Ca^{2+}]_c$ resting level.

By using a Green's function approach or the Laplacian Spectral Decomposition method, we derived *exact* formulae for the *$[Ca^{2+}]_c$ accumulation*. These formulae show explicit dependence on the diffusion constants, geometric constrains gathered in the eigenfunctions and eigenvalues $(\phi_i(x), \lambda_i)$, initial conditions, external fluxes and/or perturbations, and Ca^{2+} cycling terms proportional to $[Ca^{2+}]_c$. Interestingly, our analysis suggests that *$[Ca^{2+}]_c$ accumulation* is independent of the remaining cellular processes, so we can use our methodology even when the analytical expression for these fluxes are unknown, in contrast to the commonly used numerical simulations. We considered a finite unidimensional domain, for which the eigenfunctions and eigenvalues used in the LSD method have an analytical closed form. However, it is not always possible to achieve such expressions. Alternatively, they can be obtained numerically for complex spatial geometries by exploiting the Finite Element Method [50] and use analytical functions that numerically approximate the eigenvectors and eigenvalues.

Although a pure computational approach may yield the spatial distribution for *$[Ca^{2+}]_c$ accumulation*, it is difficult to identify the impact of the involved cellular processes on the *$[Ca^{2+}]_c$ accumulation*. In contrast, our analytical approach provides a means to link cellular processes with their impact on cytosolic Ca^{2+} accumulation. Moreover, our methodology overcomes usual problems that arise from the numerical solution of PDEs, such as accuracy errors and computational load.

We considered two biological scenarios that impel the progression of Ca^{2+} signals, namely: i) localised initial concentration of cytosolic Ca^{2+}; and ii) spatial anisotropies of extracellular Ca^{2+}. From these experiments, we noted that

- downstream signalling remains localised to the original location of the initial Ca^{2+} distribution under immobile Ca^{2+} buffers. Therefore, creating calcium microdomains and potentially triggering downstream phenomena in space selectively. This agrees with observations that release of Ca^{2+} by the endoplasmic reticulum remains confined close to IP_3 and ryanodine receptors.
- Moreover, the fluctuations of extracellular Ca^{2+} will yield an effect on the intracellular $[Ca^{2+}]_c$, yet the diffusion of species will act as a low-pass filter that vanishes the effect of higher order harmonics, potentially reducing the impact of fast stochastic fluctuations. Therefore, in order to promote Ca^{2+} microdomains, nearby cells releasing calcium may need to sustain Ca^{2+} signals with low spatial frequency for a period of time.

We foresee that the methodology presented here will aid on the analysis of a broader range of stimulus and, consequently, for more specific physiological phenomena.

APPENDIX A

Green's Function for BVP in Eq. (24)

In this section, we obtain the solution of $g(x,\xi)$ that satisfies the boundary value problem in (24). First, we note that close to the boundaries of the spatial domain $\delta(x-\xi)=0$. Hence, in the vicinity of the boundaries, $g(x,\xi)$ is the solution of a second order, linear, unforced ODE. This solution is given by

$$g(x,\xi)=\begin{cases} c_0(\xi)\cosh(\theta x)+c_1(\xi)\theta^{-1}\sinh(\theta x), \\ \qquad \text{close to } x=0, \\ c_2(\xi)\cosh(\theta[x-L])+c_3(\xi)\theta^{-1}\sinh(\theta[x-L]), \\ \qquad \text{close to } x=L. \end{cases} \tag{46}$$

By differentiating the equation above and considering the no-flux boundary conditions in (24b), we conclude that

$$c_1(\xi)=c_3(\xi)=0. \tag{47}$$

In addition to satisfying the boundary conditions, the Green's function $g(x,\xi)$ is a continuous function of x and ξ, especially at $x=\xi$ [40]. That is, from (46) and taking into account (47), $g(\xi,\xi)$ satisfies

$$c_0(\xi)\cosh(\theta\xi)=c_2(\xi)\cosh(\theta[\xi-L]).$$

However, the derivative of $g(x,\xi)$ w.r.t x evaluated at the $x=\xi$, must be a discontinuous function [40]:

$$c_0(\xi)\,\theta\sinh(\theta\xi)-c_2(\xi)\theta\sinh(\theta[\xi-L])=1.$$

By combining the two last expressions we obtain the algebraic system

$$\begin{pmatrix} \cosh(\theta\xi) & -\cosh(\theta[\xi-L]) \\ \theta\sinh(\theta\xi) & -\theta\sinh(\theta[\xi-L]) \end{pmatrix}\begin{pmatrix} c_0(\xi) \\ c_2(\xi) \end{pmatrix}=\begin{pmatrix} 0 \\ 1 \end{pmatrix},$$

whose solution is

$$\begin{pmatrix} c_0(\xi) \\ c_2(\xi) \end{pmatrix}=\frac{1}{\theta\sinh(\theta L)}\begin{pmatrix} \cosh(\theta[\xi-L]) \\ \cosh(\theta\xi) \end{pmatrix}.$$

By substitution of the solutions for $c_i(\xi)$ above and in (47) into (46), the to the Green's function becomes

$$g(x,\xi)=\frac{1}{\theta\sinh(\theta L)}\times\begin{cases} \cosh(\theta[\xi-L])\cosh(\theta x), & 0\le\xi<x, \\ \cosh(\theta\xi)\cosh(\theta[x-L]), & x\le\xi\le L. \end{cases}$$

APPENDIX B

Solution for $I(c_c)(x)$ with $f(x)$ as in Eq. (40)

Let us consider now the forcing function in (40) so as to evaluate the integral in (28a) for the interval $x\in[\frac{L}{2}-\varepsilon,\frac{L}{2}]$. This derivation is given as follows:

$$
\begin{aligned}
I(c_c)(x) &= \int_{\frac{L}{2}-\varepsilon}^{\frac{L}{2}} g_s(x,\xi) f(\xi)\mathrm{d}\xi, \\
&= \frac{\psi}{\theta D_c \sinh\left(\theta\frac{L}{2}\right)} \int_{\frac{L}{2}-\varepsilon}^{x} \cosh\left(\left[x-\frac{L}{2}\right]\right)\cosh(\theta\xi)\mathrm{d}\xi \\
&\quad + \frac{\psi}{\theta D_c \sinh\left(\theta\frac{L}{2}\right)} \int_{x}^{\frac{L}{2}} \cosh\left(\theta\left[\xi-\frac{L}{2}\right]\right)\cosh(\theta x)\mathrm{d}\xi \\
&= \frac{\psi}{\theta^2 D_c \sinh\left(\theta\frac{L}{2}\right)} \cosh\left(\theta\left[x-\frac{L}{2}\right]\right) \\
&\quad \cdot \left[\sinh(\theta x) - \sinh\left(\theta\left[\frac{L}{2}-\varepsilon\right]\right)\right] \\
&\quad - \frac{\psi}{\theta^2 D_c \sinh\left(\theta\frac{L}{2}\right)} \cosh(\theta x)\sinh\left(\theta\left[x-\frac{L}{2}\right]\right) \\
&= \frac{\psi}{\alpha}\left[1 - \frac{\sinh\left(\theta\left[\frac{L}{2}-\varepsilon\right]\right)}{\sinh\left(\theta\frac{L}{2}\right)} \cosh\left(\theta\left[x-\frac{L}{2}\right]\right)\right], \\
&\quad x \in \left[\frac{L}{2}-\varepsilon, \frac{L}{2}\right].
\end{aligned}
\tag{48}
$$

There, we used the definition $\theta := \sqrt{\alpha/D_c}$. Also, we used the identities

$$
\begin{aligned}
1 &= \cosh^2(x) - \sinh^2(x), \\
\sinh(x+y) &= \sinh(x)\cosh(y) + \cosh(x)\sinh(y), \\
\cosh(x+y) &= \cosh(x)\cosh(y) + \sinh(x)\sinh(y).
\end{aligned}
$$

Now, for the interval $x \in [0, L/2-\varepsilon)$, we have to satisfy the boundary value problem in (22). In this interval $f(x) = 0$ and the solution for (22a) with the no-flux boundary condition at $x = 0$ is given by

$$
I(c_c)(x) = c_4 \cosh(\theta x), \quad x \in \left[0, \frac{L}{2}-\varepsilon\right], \tag{49}
$$

as we noted earlier during the derivation of $g(\circ)$. To ensure continuity of the solution for all x, we finally require the right and left limits of $I(c_c)(x)$ as x tends to $\frac{L}{2}-\varepsilon$ to be equal. By evaluating the equation above and (48) at $x = \frac{L}{2}-\varepsilon$ we can show that continuity is guaranteed by

$$
c_4 = \frac{\psi}{\alpha \cosh\left(\theta\left[\frac{L}{2}-\varepsilon\right]\right)}\left[1 - \frac{\sinh\left(\theta\left[\frac{L}{2}-\varepsilon\right]\right)}{\sinh\left(\theta\frac{L}{2}\right)}\cosh(\theta\varepsilon)\right].
$$

Summarising and considering the solution $I(c_c)(x)$ in the full spatial domain $[0, L]$ with symmetry w.r.t. the axis $x = L/2$, the integrated accumulation of Ca^{2+} is given by

$$
I(c_c)(x) = \frac{\psi}{\alpha} \times \begin{cases} 1 - \frac{\sinh(\theta[L/2-\varepsilon])}{\sinh(\theta L/2)}\cosh\left(\theta\left[x-\frac{L}{2}\right]\right), & \left|x-\frac{L}{2}\right| \le \varepsilon, \\ \varrho \cosh\left(\theta\left[\left|x-\frac{L}{2}\right| - \frac{L}{2}\right]\right), & \left|x-\frac{L}{2}\right| > \varepsilon, \end{cases}
$$

where $\varrho := c_4 \frac{\alpha}{\psi}$.

ACKNOWLEDGMENTS

The authors would like to thank Febe Francis for many stimulating discussions on Ca^{2+} homoeostasis. Diego A. Oyarzún acknowledges the support of the Imperial College London Junior Research Fellowship Scheme. Richard H. Middleton and Míriam R. García acknowledge the support by Science Foundation Ireland via grant 07/ IN.1/I1838.

REFERENCES

[1] M. J. Berridge, M. D. Bootman, and H. L. Roderick, "Calcium signalling: Dynamics, homeostasis and remodelling," *Nat. Rev. Mol. Cell Biol.*, vol. 4, no. 7, pp. 517–529, 2003.

[2] H. Schulman, "Calcium regulation of cytosolic enzymes," in *Integrative Aspects of Calcium Signalling*, A. Verkhratsky and E. C. T. Toescu, eds., New York, NY, USA: Plenum Press, 1998, pp. 35–233.

[3] R. Sattler and M. Tymianski, "Molecular mechanisms of calcium-dependent excitotoxicity," *J. Mol. Med.*, vol. 78, no. 1, pp. 3–13, 2000.

[4] P. Nicotera and S. Orrenius, "The role of calcium in apoptosis," *Cell Calcium*, vol. 23, no. 2, pp. 173–180, 1998.

[5] R. Rizzuto, P. Pinton, D. Ferrari, M. Chami, G. Szabadkai, P. Magalhaes, F. Di Virgilio, and T. Pozzan, "Calcium and apoptosis: Facts and hypotheses," *Oncogene*, vol. 22, no. 53, pp. 8619–8627, 2003.

[6] Z. Dong, P. Saikumar, J. Weinberg, and M. Venkatachalam, "Calcium in cell injury and death*," *Annu. Rev. Pathol. Mech. Dis.*, vol. 1, pp. 405–434, 2006.

[7] M. Rehm, H. Huber, H. Dussmann, and J. Prehn, "Systems analysis of effector caspase activation and its control by X-linked inhibitor of apoptosis protein," *Eur. Mol. Biol. Org. J.*, vol. 25, pp. 4338–4349, 2006.

[8] F. Tang and W. Liu, "An age-dependent feedback control model of calcium dynamics in yeast cells," *J. Math. Biol.*, vol. 60, no. 6, pp. 849–879, 2010.

[9] S.-Y. Shin, S.-M. Choo, S.-H. Woo, and K.-H. Cho, "Cardiac systems biology and parameter sensitivity analysis: Intracellular Ca2+ regulatory mechanisms in mouse ventricular myocytes,"in *Protein–Protein Interaction*. New York, NY, USA: Springer, 2008, vol. 110, pp. 25–45.

[10] F. Francis, M. R. García, and R. H. Middleton, "A single compartment model of pacemaking in dissasociated substantia nigra neurons," *J. Comput. Neurosci.*, vol. 35, pp. 1–22, 2013.

[11] V. Volpert and S. Petrovskii, "Reaction-diffusion waves in biology," *Phys. Life Rev.*, vol. 6, no. 4, pp. 267–310, Dec. 2009.

[12] J. Munoz-Garcia, Z. Neufeld, and B. N. Kholodenko, "Positional information generated by spatially distributed signaling cascades," *PLoS Comput. Biol.*, vol. 5, no. 3, p. e1000330, Mar. 2009.

[13] B. S. Gardiner, L. Zhang, D. W. Smith, P. Pivonka, and A. J. Grodzinsky, "A mathematical model for targeting chemicals to tissues by exploiting complex degradation," *Biol. Direct*, vol. 6, p. 46, Sep. 2011.

[14] F. López-Caamal, M. R. García, R. H. Middleton, and H. J. Huber, "Positive feedback in the Akt/mTOR pathway and its implications for growth signal progression in skeletal muscle cells: An analytical study," *J. Theor. Biol.*, vol. 301, pp. 15–27, May 2012.

[15] K. L. Engisch and M. C. Nowycky, "Calcium dependence of large dense-cored vesicle exocytosis evoked by calcium influx in bovine adrenal chromaffin cells," *J. Neurosci.*, vol. 16, no. 4, pp. 1359–1369, 1996.

[16] C. Schofl, G. Brabant, R.-D. Hesch, A. von zur Muhlen, P. H. Cobbold, and K. Cuthbertson, "Temporal patterns of alpha 1-receptor stimulation regulate amplitude and frequency of calcium transients," *Am. J. Physiol.-Cell Physiol.*, vol. 265, no. 4, pp. C1030–C1036, 1993.

[17] B. Milojkovic, W. Zhou, and S. Antic, "Voltage and calcium transients in basal dendrites of the rat prefrontal cortex," *J. Physiol.*, vol. 585, no. 2, pp. 447–468, 2007.

[18] C. Vahl, A. Bonz, T. Timek, and S. Hagl, "Intracellular calcium transient of working human myocardium of seven patients transplanted for congestive heart failure," *Circulation Res.*, vol. 74, no. 5, pp. 952–958, 1994.

[19] J. Deshpande, B. Siesjo, and T. Wieloch, "Calcium accumulation and neuronal damage in the rat hippocampus following cerebral ischemia," *J. Cerebral Blood Flow Metabolism*, vol. 7, no. 1, pp. 89–95, 1987.

[20] R. Heinrich, B. G. Neel, and T. A. Rapoport, "Mathematical models of protein kinase signal transduction," *Mol. Cell*, vol. 9, no. 5, pp. 957–970, May 2002.

[21] J. Keener and J. Sneyd, *Mathematical Physiology: Cellular Physiology*, vol. 1., New York, NY, USA: Springer, 2009.
[22] R. Courant and D. Hilbert, *Methods of Mathematical Physics*. Hoboken, NJ, USA: Wiley, 1937.
[23] A. A. Alonso and B. Ydstie, "Stabilization of distributed systems using irreversible thermodynamics," *Automatica*, vol. 37, no. 11, pp. 1739–1755, 2001.
[24] F. López-Caamal, M. R. García, D. A. Oyarzun, and R. H. Middleton, "Analytic computation of the integrated response in nonlinear reaction-diffusion systems," in *Proc. IEEE 51st Annu. Conf. Decision Control*, 2012, pp. 1047–1052.
[25] D. A. Oyarzún, F. López-Caamal, M. R. García, R. H. Middleton, and A. Y. Weiße, "Cumulative signal transmission in nonlinear reaction-diffusion networks," *PLoS ONE*, vol. 8, no. 5, pp. e62 834, May 2013.
[26] G.-F. Tian, H. Azmi, T. Takano, Q. Xu, W. Peng, J. Lin, N. Oberheim, N. Luo, X. Wang, and H. Zielke, "An astrocytic basis of epilepsy," *Nature Med.*, vol. 11, no. 9, pp. 973–981, 2005.
[27] N. J. Allen and B. A. Barres, "Neuroscience: Glia–More than just brain glue," *Nature*, vol. 457, no. 7230, pp. 675–677, Feb. 2009.
[28] T. Fellin, O. Pascual, and P. G. Haydon, "Astrocytes coordinate synaptic networks: Balanced excitation and inhibition," *Physiol.*, vol. 21, no. 3, pp. 208–215, 2006.
[29] H. Kettenmann and A. Verkhratsky, "Neuroglia: The 150 years after," *Trends Neurosci.*, vol. 31, no. 12, pp. 653–659, 2008.
[30] M. Oheim, F. Kirchhoff, and W. Stühmer, "Calcium microdomains in regulated exocytosis" *Cell Calcium*, vol. 40, nos. 5–6, pp. 423–439, 2006.
[31] A. Fanelli, J. I. Titapiccolo, F. Esposti, M. Ripamonti, A. Malgaroli, and M. G. Signorini, "Novel image processing methods for the analysis of calcium dynamics in glial cells," *IEEE Trans. Biomed. Eng.*,, vol. 58, no. 9, pp. 2640–2647, Sep. 2011.
[32] M. Santello, C. Calì, and P. Bezzi, "Gliotransmission and the tripartite synapse," in *Synaptic Plasticity*, New York, NY, USA: Springer, 2012, pp. 307–331.
[33] R. Thul, G. Smith, and S. Coombes, "A bidomain threshold model of propagating calcium waves," *J. Math. Biol.*, vol. 56, no. 4, pp. 435–463, 2008.
[34] Z. Zhou and E. Neher, "Mobile and immobile calcium buffers in bovine adrenal chromaffin cells," *J. Physiol.*, vol. 469, no. 1, pp. 245–273, 1993.
[35] A. Verkhratsky and E. Toescu, *Integrative Aspects of Calcium Signalling*. New York, NY, USA: Springer, 1998.
[36] A. Korngreen, V. Goldshtein, and Z. Priel, "A realistic model of biphasic calcium transients in electrically nonexcitable cells," *Biophys. J.*, vol. 73, no. 2, pp. 659–673, 1997.
[37] E. Yanagida, S. Shoji, Y. Hirayama, F. Yoshikawa, K. Otsu, H. Uematsu, M. Hiraoka, T. Furuichi, and S. Kawano, "Functional expression of Ca2+ signaling pathways in mouse embryonic stem cells," *Cell Calcium*, vol. 36, no. 2, pp. 135–146, 2004.
[38] M. Sedova and L. A. Blatter, "Dynamic regulation of [Ca2+]iby plasma membrane Ca2+-atpase and Na+/Ca2+exchange during capacitative Ca2+entry in bovine vascular endothelial cells," *Cell Calcium*, vol. 25, pp. 333–343, May 1999.
[39] D. Gill, S. Chueh, and C. Whitlow, "Functional importance of the synaptic plasma membrane calcium pump and sodium-calcium exchanger," *J. Biol. Chem.*, vol. 259, no. 17, pp. 10807–10813, 1984.
[40] I. Stakgold, *Green's Functions and Boundary Value Problems*. Hoboken, NJ, USA: Wiley, 1979.
[41] J. Wagner and J. Keizer, "Effects of rapid buffers on Ca2+ diffusion and Ca2+ oscillations," *Biophys. J.*, vol. 67, no. 1, pp. 447–456, 1994.
[42] N. A. Oberheim, T. Takano, X. Han, W. He, J. H. Lin, F. Wang, Q. Xu, J. D. Wyatt, W. Pilcher, J. G. Ojemann, B. R. Ransom, S. A. Goldman, and M. Nedergaard, "Uniquely hominid features of adult human astrocytes," *J. Neurosci.*, vol. 29, no. 10, pp. 3276–3287, 2009.
[43] N. Pivovarova, H. Nguyen, C. Winters, C. Brantner, C. Smith, and S. Andrews, "Excitotoxic calcium overload in a subpopulation of mitochondria triggers delayed death in hippocampal neurons," *J. Neurosci.*, vol. 24, no. 24, pp. 5611–5622, 2004.
[44] L. Guo and R. Davidson, "Extracellular Ca2+ increases cytosolic free Ca2+ in freshly isolated rat odontoblasts," *J. Bone Miner. Res.*, vol. 14, no. 8, pp. 1357–1366, 1999.
[45] V. De Arcangelis, D. Coletti, M. Canato, M. Molinaro, S. Adamo, C. Reggiani, and F. Naro, "Hypertrophy and transcriptional regulation induced in myogenic cell line l6-c5 by an increase of extracellular calcium," *J. Cell. Physiol.*, vol. 202, no. 3, pp. 787–795, 2005.
[46] M. Persson-Rothert, J. Egas-Kenniphaas, E. Valk-Kokshoorn, J. Buys, and A. Laarse, "Oxidative stress-induced perturbations of calcium homeostasis and cell death in cultured myocytes: Role of extracellular calcium," *Mol. Cell. Biochem.*, vol. 136, no. 1, pp. 1–9, 1994.
[47] A. Schousboe and H. Waagepetersen, "Role of astrocytes in glutamate homeostasis: Implications for excitotoxicity," *Neurotoxicity Res.*, vol. 8, pp. 221–225, 2005.
[48] D. Friedmann-Morvinski, E. A. Bushong, E. Ke, Y. Soda, T. Marumoto, O. Singer, M. H. Ellisman, and I. M. Verma, "Dedifferentiation of neurons and astrocytes by oncogenes can induce gliomas in mice," *Science*, vol. 338, no. 6110, pp. 1080–1084, 2012.
[49] R. B. Silver, "Calcium, BOBs, QEDs, microdomains and a cellular decision: Control of mitotic cell division in sand dollar blastomeres," *Cell Calcium*, vol. 20, no. 2, pp. 161–179, 1996.
[50] M. R. García, C. Vilas, J. R. Banga, and A. A. Alonso, "Optimal field reconstruction of distributed process systems from partial measurements," *Ind. Eng. Chem. Res.*, vol. 46, no. 2, pp. 530–539, 2007.

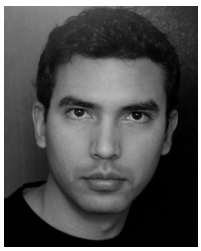

Fernando López-Caamal graduated as a mechatronic engineer in 2007 and received the master's degree in control engineering in 2009, both from the Universidad Nacional Autónoma de México. In 2013, he received the PhD degree from the National University of Ireland, Maynooth. His research interests include mathematical analysis and modelling of biochemical and genetic networks.

Diego A. Oyarzún received the licenciatura and magíster degrees in electronic engineering from the Universidad Técnica Federico Santa María, Chile, in 2006, and the PhD degree from the National University of Ireland, Maynooth, in 2010. Since 2013, he has been a junior research fellow in biomathematics at Imperial College London, where he develops novel mathematical approaches for the analysis and design of biomolecular networks.

Richard H. Middleton received the PhD degree from the University of Newcastle, Australia, in 1987. He was a research professor at the Hamilton Institute, The National University of Ireland, Maynooth from May 2007 to 2011 and is currently a professor at the University of Newcastle and the director of the Priority Research Centre for Complex Dynamics Systems and Control. He has served as program chair (CDC 2006), CSS Vice President Membership Activities, and the Vice President Conference Activities. In 2011, he was the president of the IEEE Control Systems Society. His research interests include control systems theory and applications, including robotics, control of distributed systems and systems biology with applications to Parkinson's disease and HIV dynamics. He is a fellow of the IEEE and IFAC.

Míriam R. García studied chemistry from the University of Vigo and received the PhD degree in applied mathematics from the same university. She was a postdoctoral researcher for more than five years in the Systems Biology Department at the Hamilton Institute, National University of Ireland, Maynooth. She is currently in the Process Engineering Group belonging to the Spanish National Research Council (IIM-CSIC). She has more than 10 years of research experience and her research interests include distributed process systems, theoretical biology, and food and biotechnology processes.